Urban Forestry & Urban Greening 46 (2019) 126513

Contents lists available at ScienceDirect

Urban Forestry & Urban Greening

journal homepage: www.elsevier.com/locate/ufug

Using 3D digital image correlation in an identification of defects of trees subjected to bending

Jan Tippner[a], Luděk Praus[a], Martin Brabec[a], Václav Sebera[a,b,c,*], Barbora Vojáčková[a], Jaromír Milch[a]

[a] Department of Wood Science, Mendel University in Brno, Brno, 61300, Czech Republic
[b] InnoRenew CoE, Izola, 6310, Slovenia
[c] University of Primorska, Koper, 6000, Slovenia

ARTICLE INFO

Handling Editor: Richard Hauer

Keywords:
Arboriculture
Optical non-contact assessment
Pulling test
Strain
Tree defect
Tree-root system

ABSTRACT

Abrupt changes of climate have intensified during the last few decades, bringing higher risks from tree failures by either uprooting or stem breakage. To eliminate the risks, many techniques of tree assessment are being used. In the presented work, an optical technique based on 3D Digital Image Correlation (3D-DIC) was investigated as one of the tools to be used in identification of tree defects. Within the work, two ash trees were examined by pulling tests coupling 3D-DIC and standard techniques. The trees were measured in five consecutive steps of artificially made defects of two kinds - root and stem damage. We hypothesized defects can be identified using full-field strains and displacements. Results indicated that 3D-DIC provides comparable strains as standard semi-destructive extensometers. Statistical tests ($\alpha = 0.05$) showed the 3D-DIC technique method is capable of identifying changes of displacements and strains after creating artificial defects in trees. However, despite the statistical differences, the practical arboricultural considerations of findings are still limited due to low absolute differences. The study also suggests there might exist path-dependency of the defect creation order when evaluating stiffness/strains from extensometers of two different positions. This could have impact on a practical assessment of tree stability in the future, but it must be further tested on larger data sets due to the proof-of-concept character of this work. In general, 3D-DIC brings extensive improvement in data acquisition quality and quantity, especially from the perspective of natural variability and heterogeneity in trees and wood.

1. Introduction

During the last decades, people have been facing more abrupt changes of weather including wind and rain/snow storms (Quine, 1995; Schelhaas et al., 2003). A more frequent occurrence of catastrophic wind storms attributed to climatic change is supposed to increase in the future (Seidl et al., 2014, Pachauri and Meyer 2014, IPCC, 2014). These events bring direct damage of trees, loss of timber, damage to properties, power outages, reduction in the carbon sink due to the loss of forest area, loss of ecosystem services, or even fatalities (Gardiner, 2013; Dahle et al. 2017b; Chirici et al., 2018). Due to these facts, the role of foresters and arborists, who are involved in tree management or stability assessment to various degrees, has become more required and more sophisticated from a techniques-to-be-used perspective (Lindroth et al., 2009; Schmidlin, 2009). To assess tree stability, a whole variety of techniques can be used, ranging from only qualitative, mainly visual approaches such as visual tree assessment (VTA) and statics integrating assessment (SIA), to quantitative ones (Mattheck, 2004). The latter enable determination of the probability of failure through safety factors (Niklas and Spatz, 2000). Calculation of factors is based on comparison between measured parameters on trees and wood properties or empirically determined criteria (Peltola, 2006; Dahle et al., 2017a).

Among quantitative techniques, pulling tests are predominantly used in arboriculture and urban forestry to determine tree mechanical response to loading and, consequently, its stability. The pulling test has been widely used since the early sixties (Fraser, 1962) and was well documented during the last decades (Wessolly, 1991; Brudi and Wassenaer, 2001; Detter, 2012). The pulling test belongs to functional techniques since it examines the mechanical functionality of a tree (Mancuso, 2012). The basic principle of the pulling test is simultaneous measurement of acting force, stem base rotation, and stem deformation using various types of extensometers or strain gauges. Stem base rotation is mainly correlated with failure loads and turning moments (Peltola, 2006; Lundstrom et al., 2007; Ghani et al., 2008) or with

* Corresponding author at: Bruzovská 1844, Frýdek-Místek, 738 01, Czech Republic.
E-mail address: vaclav.sebera@mendelu.cz (V. Sebera).

https://doi.org/10.1016/j.ufug.2019.126513
Received 3 May 2018; Received in revised form 24 October 2019; Accepted 27 October 2019
Available online 03 November 2019

empirically determined functions determined by the research community (Brudi and Wassenaer, 2001; Sani et al., 2012; Szórádová et al., 2013; Buza and Divos, 2016). Stem deformation is generally used for assessment of resistance to stem breakage by comparison with material properties (Brudi and Wassenaer, 2001; Dahle et al., 2017a). Strain gauges are primarily used to obtain the strain in a stem to better understand the tree response to static loading (Ennos, 1995; Stokes, 1999; Crook and Ennos, 1996). An important outcome of the pulling test is data that enable creation of predictive models for tree failure with respect to tree parameters. A predictive model of vertical uprooting using Bayesian inference was given by Yan et al. (2016).

Recently, there have been efforts to implement non-contact optical techniques based on digital image correlation (DIC) in trees' assessment to provide displacements, strains, and rotations at the tree surface during a pulling test (NASA, 2013; Sebera et al., 2014, 2016). Stereoscopic form of DIC (3D-DIC) is a technique that is capable of capturing displacements and strains on the curved surfaces of a measured body (Peters and Ranson, 1982; Sutton et al., 2009) and, therefore, is applicable in tree biomechanics. Implementation of optical techniques into pulling tests has brought advances such as: (i) bigger data sets, implying a partial elimination of a localness of measured quantities (more parts of a tree are analyzed) and providing data in 3D (especially in full-field regime) or even 4D where time is the fourth dimension as shown for root growth analysis in Basu and Pal (2012), because from a statistical point of view, bigger data sets allow for consideration of natural and high heterogeneity and variability of tree tissues (Gryc and Vavrčík, 2009; Longuetaud et al., 2017); (ii) non-contact techniques do not harm living tree tissues; (iii) optical data further enable analysis of parts that were not analyzed for the first time during an experiment, i.e., further analysis may focus on different locations of the tree (within an image) without repeating the experiments.

The optical techniques that may be employed in tree assessment are principally of two fundamental kinds: marker-tracking and full-field analysis. Marker-tracking is especially useful for measuring whole trees, including branches, either dynamically or statically loaded (James et al., 2006). This may conveniently lead to a derivation of the tree deflection line. The full-field regime is convenient for an analysis of tree detail since it provides millions of measuring points. The already mentioned efforts were focused on applicability of the 3D-DIC technique in tree assessment. More recent works concentrated on assessment of the influence of bark on strain transfer from xylem to bark since the optical measurement provides data only on tree surfaces. Sebera et al. (2016) showed that displacements of bark and xylem at middle-size trees (approx. 28 cm in diameter) correlate immediately, even at low loads, but strains start to be statistically equivalent only after reaching a certain load (approx. 5 kN). However, Dahle (2017b) showed that for thinner branches (approx. 3–4 cm in diameter) it is not necessary to remove bark to investigate strains in xylem because strains on both tissues were comparable. This further develops findings of Niklas (1999) who found out that mechanical contribution of bark cannot be neglected for young trees.

With respect to this paper, Ciftci et al. (2014) investigated an effect of stem decay representing a certain cavity, on a moment capacity of tree stems. The authors simulated cavities by artificially made notches in a tree stem and found significant decrease of moment capacity and shift of a neutral axis. One of the objectives in tree assessment is to identify and explore potential internal defects. For this defectoscopic purpose, several techniques are currently used such as acoustic and electric tomography and resistography (Brazee et al., 2011; Gao et al., 2017). Functional methods do not allow detection of spatial extent of the defect, but the change (usually loss) of function such as stiffness and strength of the stem or branch. From a mechanical point of view, there hasn't been study focusing on investigation of tree internal defects using optical techniques such as DIC.

Hence, to address this research question, the specific goals of this proof-of-concept study are as follows: (a) to carry out defect-free tree pulling tests while using both standard techniques and optical full-field techniques to measure strain induced in a tree and compare both approaches; (b) to investigate whether it is possible to identify artificially made defects of tree stem and roots using optical techniques based on DIC; (c) to assess the failure of the trees using standard strain measurement techniques.

2. Methods

2.1. Pulling test

Two ash trees (*Fraxinus excelsior* L.) were tested using pulling test assisted with stereoscopic video-camera set. The trees grew in a floodplain forest stand with dominance of European ash close to Rajhrad, South Moravia, Czech Republic. Altitude of the site is 200 m a.s.l., average temperature is 9–10 °C, and the average annual rainfall is between 450 and 500 mm. The height of measured trees was 36 m and diameter at breast height (DBH) was 38 cm and 41 cm, respectively.

The pulling force was induced using Yaletrac cable puller Y32 with nominal force 32 kN. The force was measured using Isetron M-0060-1/N load cell with measuring range 0–50 000 N and accuracy 100 N. The pulling test was performed only in the range of elastic deformation that was controlled by the measurement of the stem wood strain up to 0.1% and stem base rotation up to 0.1°. During the test, both mechanical and optical set were employed to measure displacements and strains on bark. The mechanical set included two inductive linear variable displacement transducers (LVDT), the Mesing T101 F produced by Mesing Ltd. with measuring range of ± 2 mm and sensitivity of 0.001 mm, with special housing, placed in position 0.5 and 1.4 m above the ground on the compression side of the stem. The LVDTs were attached to trees using screws to obtain good connection with the xylem. Depth of penetration was approximately 2 cm. Stem base inclination was monitored using two Sitall STS-001-1-10-I inclinometers with measuring range ± 5 degrees and sensitivity 0.05%. The data were collected using a DEWE43 data-logger manufactured by DEWETRON (Elektronische Messgeräte GmbH). The acquisition frequency was set to 10 Hz and was controlled by Dewesoft 7.0 installed at a controlling laptop.

Next to the tree, the optical stereoscopic video-camera set for obtaining images for subsequent 3D-DIC computation was placed (Fig. 1). The 3D-DIC set was focused on an area of interest (AoI) that included artificial defect made from the other side of the tree stem (Fig. 1). The set consisted of two CCD cameras, Allied AVT – Stingray, each with a resolution of 2452 × 2056 p × . The sufficient depth of field capable to fully cover the AoI shape was obtained by using lenses with a focal length of 25 mm and appropriate aperture diaphragm. The distance of cameras from the captured AoI was approximately 140 cm, which resulted in a scale of 3.2 px/mm. An acquisition rate was set to 1 Hz. Before acquisition of images, the set was calibrated to obtain the stereoscopic view on the AoI. The calibration was carried out with help of a sequence of 20 calibration images containing a calibration grid at different angles and spatial positions in respect to the sensor plane of cameras (for more see Sebera et al., 2014). All captured images were 8bit with standard grey scaling of 256 levels. The displacement and strain field was computed using 3D-DIC algorithm implemented in Vic-2010 software (Correlated Solutions Ltd.). In order to obtain the maximal spatial resolution of strain field, the lowest possible strain filter size of 5 × 5 points was applied. In order to reduce an average computational error up to 0.01 px over AoI, a subset size of 81 × 81 px was used. A subset step of 5 px provided the optimal ratio between the density of correlated points and the computing time. The AoI was conveniently prepared for DIC analysis by applying a stochastic and unique black-and-white pattern all over it using chalk sprays. To assure sufficient contrast between pattern components and to suppress an effect of sun and clouds, the AoI was lit by LED-chip lights, each having luminous flux about 17 000 cd.

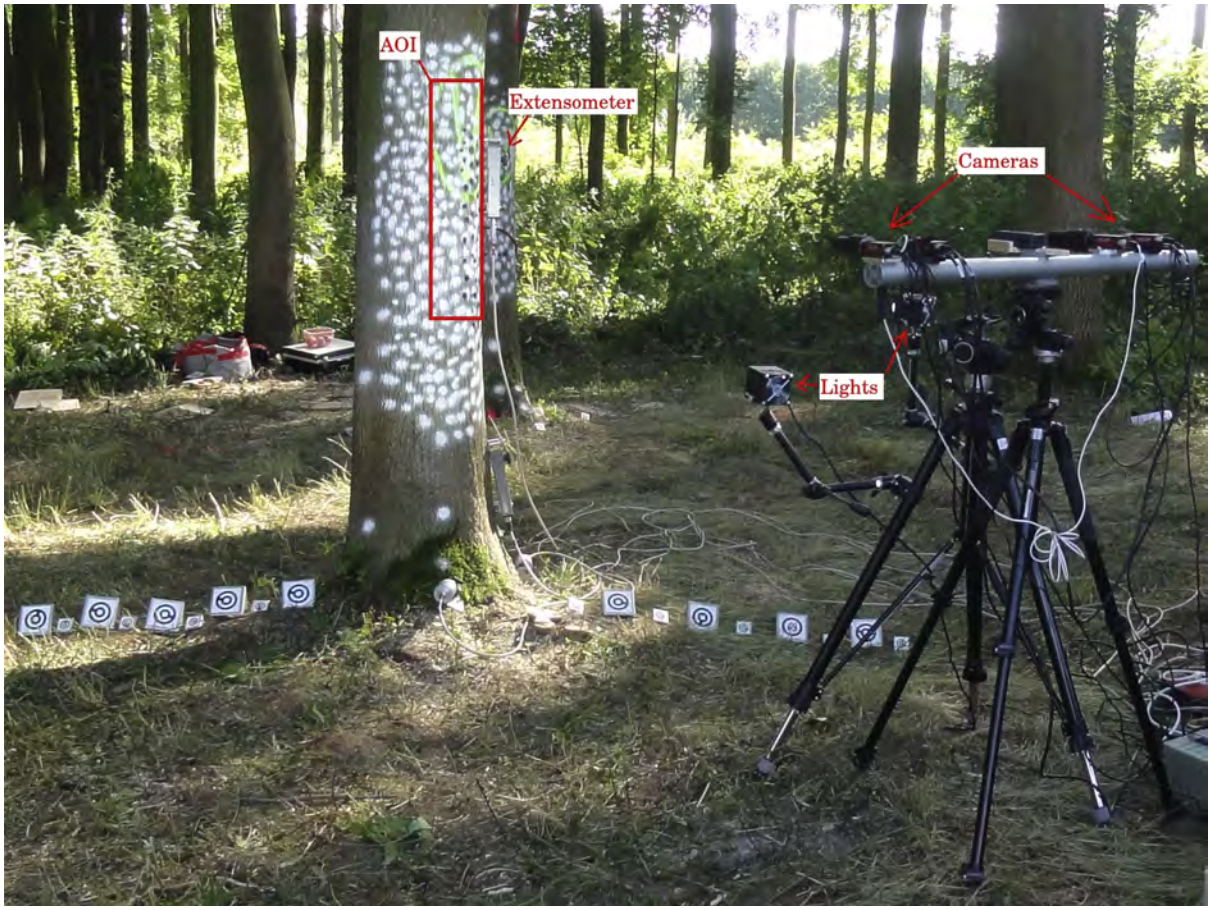

Fig. 1. Measurement setup at tree 1: stereoscopic video-camera set for image acquisition for subsequent 3D-DIC analysis.

2.2. Experimental procedure

The force was applied in an angle of 50° with respect to the area of interest (AoI, see Fig. 1); a rope was attached to the tree at a height of 15 m and an inclination of 28° and 31.5°, respectively. Experiments consisted of set of measurements on two trees at various stem and root damage level. During every measurement, the pulling test was carried out while using both standard and optical techniques (Fig. 1). Both trees were damaged in five levels, but in a different order: Tree 1was first damaged in roots and then in stem; Tree 2 was first damaged in stem and then in roots. Details of damage order is shown in Table 1.

The root damage was made by a digger, resulting in excavations 120 cm deep in distances of 3 m and 1 m from the tree base. The excavation was made on the opposite side of the pulling rope only. The stem damage was made using a chainsaw creating rectangular holes located at the tree stem at the opposite side to the AoI (Fig. 2). The sizes of the stem damages for tree 1 are as follows: SD1 = 25×15×17 cm^3 (length × width × depth); SD2 = 45×15×25 cm^3 and SD3 = 76×15×25 cm^3; the sizes of the stem damages for the tree 2 are following: SD1 = 23×14×20 cm^3 (length × width × depth); SD2 = 48×14×28 cm^3 and SD3 = 77×14×38 cm^3. After all six pulling tests on each tree that were coupled with the optical set, complete destructive pulling tests (with failure) were carried out for both trees. For these tests, the optical set was not used but only standard equipment such as extensometers, inclinometers, and load cell. The objective of these tests was to observe the character of a failure.

Using 3D-DIC (VIC-3D) resulted in obtaining full-field data on a tree bark. These data consisted of displacement vector components (*U*, *V* and *W*) and 2D strain tensor (ε_{xx}, ε_{yy} and ε_{xy}). These full-field data were processed in the form of box-plots and were further statistically tested by multiple comparison ANOVA tests at significance level of $\alpha = 0.05$. All tests with full-field data were carried out in Matlab 2014b (Mathworks Inc., USA). The statistical testing of slopes was carried out using Matlab functions (*aoctool* and *multcompare*) for analysis of covariance (ANCOVA) and analysis of variance (ANOVA), both at the $\alpha = 0.05$. The data from pointwise inspections in the computed fields, such as virtual extensometers, were processed by Microsoft Excel 2010 (Microsoft Corporation Inc.).

3. Results and discussion

The main goal of this work was to investigate whether 3D-DIC technique can be used to identify or detect an artificially made damage to a tree when compared to its non-damaged state. Therefore, the responses of two ash trees (*Fraxinus excelsior* L.) loaded in bending mode were monitored using both standard and optical techniques. In order to

Table 1
Order of developing defects and measurement.

Tree 1	i) No stem and no root damage (NSD + NRD); ii) no stem damage and 1st root damage (NSD + RD1); iii) no stem damage and 2nd root damage (NSD + RD2); 1st stem damage and 2nd root damage (SD1 + RD2); iv) 2nd stem damage and 2nd root damage (SD2 + RD2); v) 3rd stem damage and 2nd root damage (SD3 + RD2).
Tree 2	i) No stem and no root damage (NSD + NRD); ii) 1st stem damage and no root damage (SD1 + NRD); iii) 2nd stem damage and no root damage (SD2 + NRD); 3rd stem damage and no root damage (SD3 + NRD); iv) 3rd stem damage and 1st root damage (SD3 + RD1); v) 3rd stem damage and 2nd root damage (SD3 + SD2).

Fig. 2. Details of the artificially made defects at tree 1: a) 1st stem damage (NRD + SD1), b) 2nd stem damage (NRD + SD2), c) 3rd stem damage (NRD + SD3), d) 1st root damage (RD1 + SD3), e) 2nd root damage (RD2 + SD3).

reach the main goal, the first objective was to assess whether the optical technique provided equivalent strain data as extensometers. The validation of the optical technique was proved by comparison of tree strains obtained by virtual extensometers within the optical 3D-DIC system and standard extensometers. In Fig. 3, comparison data from both measuring systems on an example of non-damaged state is shown. Obtained relative difference (RD) between standard extensometers and optical ones was as follows: Tree 1 exhibited mean RD = 5.0% and median RD = 2.3%; Tree 2 exhibited mean RD = 13.6% and median RD = 10.1%. Calculation of RD was carried out for strains above 0.02% (in absolute terms) to avoid difficulties with dividing by nearly-zero values and due to the noise of measurement at low strains. Therefore, we may state that in this proof-of-concept study virtual extensometers provide comparable data to ones obtained from mechanical extensometers. We see that optical setup has a lower acquisition rate than extensometers, which is given by camera parameters, but, nonetheless, it is good enough to capture the detailed deformation process induced by a pulling test of standard force rate – the wave of the deformation can be well interpreted using virtual extensometer data. Practically the same characteristics were also achieved for all other defect modes and damage levels, which are omitted here to conserve space. The absolute difference of strains obtained from virtual and standard extensometers for all damage modes was between 0.00003% (at high strains) and 0.03% (at nearly-zero strains), with average value about 0.009%.

The horizontal (ε_{xx}) and vertical (ε_{yy}) strains for both trees obtained by virtual extensometers indicated in Fig. 3 are shown in Fig. 4. For tree 1 (top row in Fig. 4), we see that stiffness expressed as force-to-strain ratio is decreasing for ε_{yy} as tree damage increases. On the contrary, such stiffness, with respect to ε_{xx}, does not reveal such a pattern. For tree 2 (bottom row in Fig. 4), stiffness related to ε_{yy} shows its decrease more clearly as tree damage increases than in the case of tree 1. For stiffness related to ε_{xx}, it revealed that as damage increased, strain had

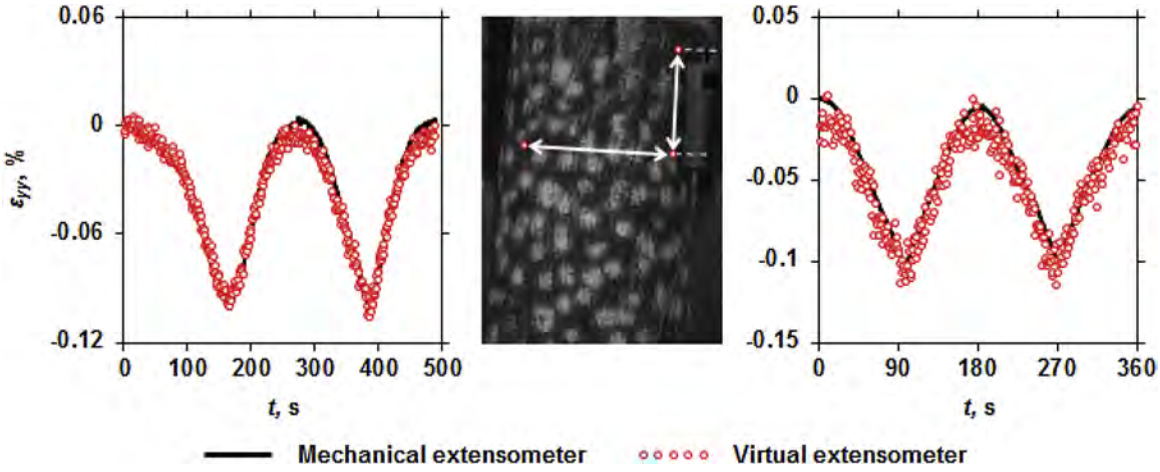

Fig. 3. Comparison of virtual and standard strain measurement techniques: normal strain in the vertical direction (ε_{yy}) on compressive sides of tree 1 (left) and tree 2 (right); the middle part shows the mechanical extensometer mounted to a tree and two virtual ones (in X and Y directions).

changed from positive values (tension) to negative ones (compression). These phenomena can be explained by possible deplanation of the cross-section of tree at defect zone and may be important from a practical point of view, too. However, it needs to be studied on bigger sample size to confirm such conclusions.

The slopes in Fig. 4 were further tested using multi-comparison ANOVA tests. The results from this testing, in a form of pairs that are not statistically different with their p values, are shown in Table 2.

Vertical strains and local relative stiffnesses (force-to-strain ratios), expressed as percentage change with respect to stiffness of non-damaged state, are shown for both trees in Fig. 5. Local relative stiffness comes from the data obtained from extensometers mounted at two different heights (E1 and E2). Fig. 5 shows that the evaluation of local relative stiffness depends on the position of extensometers. For tree 1, the E1 mounted at the tree base exhibited decrease of stiffness after root damage (RD2) but started growing as size of stem defect increased. ANOVA tests of the slopes obtained by E1 at tree 1 revealed there is no statistical difference between NSD + NRD vs. NSD + RD1 ($p = 0.99$) and between NSD + RD2 vs. SD1 + RD2 ($p = 0.28$). On the other hand, the E2 located at the stem defect zone indicates gradual reduction of local stiffness with every step of the damage, and all the slopes from the E2 are statistically different ($p < 0.05$). This means that deformation at stem defect zone is greater due to weakening of the stem cross-section; meanwhile, the deformation at the base increased after both root damages and gradually decreased after the stem damages. The stem defect zone induced "non-continues" step in deflection of the stem, as would be expected.

For tree 2, the local stiffnesses revealed different behavior than for

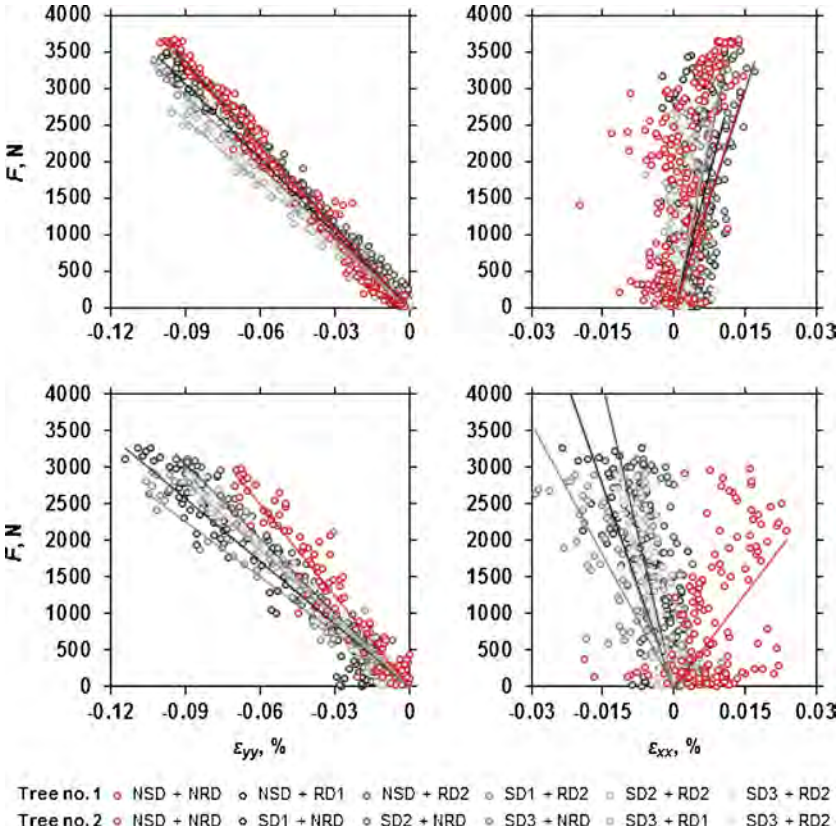

Fig. 4. Comparison of force vs. longitudinal strain (F-ε_{yy}) and force vs. transverse strain (F-ε_{xx}) characteristics in the first growing part of loading cycles of tree 1 (top row) and tree 2 (bottom row) with no defects (NSD + NRD) and with artificially made defects at different levels on tree stem (SD1-SD3) and tree roots (RD1 and RD2).

Table 2
Results from ANOVA tests for slopes shown in Fig. 4. Only pairs that do not exhibit statistical differences are listed ($p > 0.05$).

Fig. 4 upper left	All slopes are statistically different from each other.
Fig. 4 upper right	NSD + RD2 vs. SD2 + RD2 ($p = 0.41$), NSD + RD1 vs. SD2 + RD2 ($p = 0.90$), NSD + RD1 vs. NSD + RD2 ($p = 0.10$), SD1 + RD2 vs. SD3 + RD2 ($p = 1.00$)
Fig. 4 bottom left	SD1 + NRD vs. SD3 + RD1 ($p = 0.074$), SD2 + NRD vs. SD3 + NRD ($p = 0.22$), SD2 + NRD vs. SD3 + RD2 ($p = 0.097$), SD3 + NRD vs. SD3 + RD1 ($p = 0.33$), SD3 + NRD vs. SD3 + RD2 ($p = 0.99$), SD3 + RD1 vs. SD3 + RD2 ($p = 0.77$)
Fig. 4 bottom right	SD1 + NRD vs. SD3 + RD1 ($p = 0.60$), SD2 + NRD vs. SD3 + RD1 ($p = 0.84$), SD2 + NRD vs. SD3 + RD2 ($p = 0.74$), SD3 + RD1 vs. SD3 + RD2 ($p = 0.14$)

tree 1. The local stiffness at the stem defect zone (evaluated based on E2) decreased as stem damages increased but stopped decreasing with progression of root damages. On the other hand, the local stiffness at the base (evaluated based on E1) increased as size of stem defect increased but, after the first root damage (RD1), dropped and grew slightly with the second root damage (RD2). ANOVA tests of the slopes obtained by E1 at tree 2 revealed that all possible pairs are statistically different except SD3 + RD1 vs. SD3 + RD2 ($p = 0.17$). For tree 2 and E2, ANOVA showed that only pair SD3 + NRD vs. SD3 + RD2 ($p = 0.86$) is not statistically different. By comparing both trees in Fig. 5, we see that stiffness or strain evaluated at the stem defect zone and at the base of the tree may imply so-called path-dependency. This means it may depend on what kind of defect was created first, whether at a stem or at a root plate. However, this path-dependency should be proved on a bigger sample to have statistical strength since our work represents a proof-of-concept study. Interaction between the stem stiffness and root damage was also observed by Neild and Wood (1999), who predict the stiffness of a tree stem based on the root plate deflection. Nevertheless, as is evident from the results, the interaction between stem stiffness and root damage is more complex when stem defect is present. From a practical point of view, this phenomenon is not considered in a standard tree stability assessment using static integrated method where the stem deformation and root plate inclination are evaluated separately (Brudi and Wassenaer, 2001; Detter, 2012).

The advantage of application of the 3D-DIC system is that it provides full-field data, such as displacements and strains, all over the AoI. It is worth mentioning that AoI size was chosen based on apriori knowledge of defects' sizes, in many applications, it may be useful to have AoI smaller. This would increase practical potential of this technique and reduce processing of big data sets. Due to many provided results, only horizontal displacement (u) and vertical strain (ε_{yy}) are included in the article because they represent the most important results with respect to practical considerations of the pulling test. The rest of the outputs are omitted here to save space. Horizontal displacement (U) and vertical strain (ε_{yy}) field for all the damage levels of tree 2 at equivalent force levels are depicted in Fig. 6 (equivalent figure for tree 1 is omitted to save space). Even visually, we may see that maximal U increases as damage of tree root or stem becomes greater. By looking at vertical strain (ε_{yy}), we may see that the vertical strains of both trees mostly ranged from negative to approx. zero values, implying the 3D-DIC set was focused on the compression side of the trees. In Fig. 6, it is apparent that the AoI's are rather green-blue areas; nonetheless, we may conclude that strains are not easy to interpret visually and we cannot make generalizing statements. Instead, we need to inspect the AoI further using statistical methods. It is more convenient to look at median values of AoI's (Figs. 7 and 8). The statistical quantities reveal all the measured strains were lower than elastic limit of ash (~0.42% for green ash wood, Wessolly and Erb, 2016), so we may state trees

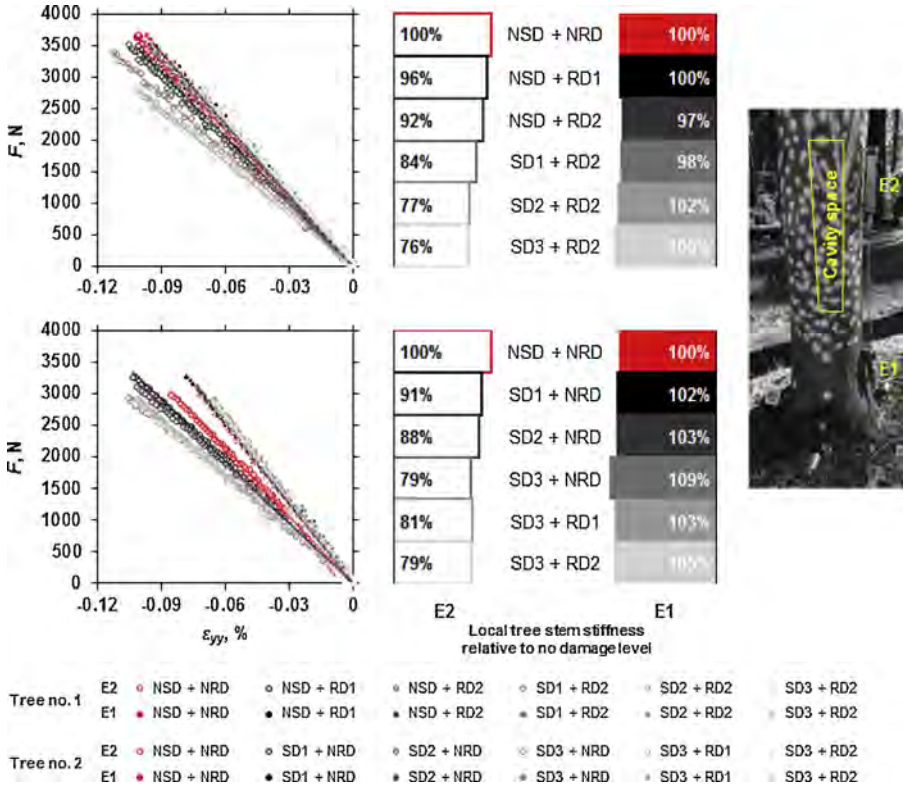

Fig. 5. Comparison of force vs. longitudinal strain (F-ε_{yy}) characteristics and local stem stiffness measured by mechanical extensometers (E1 and E2) in the 1st cycle of loading cycles of tree 1 (top row) and tree 2 (bottom row) at all levels of damage.

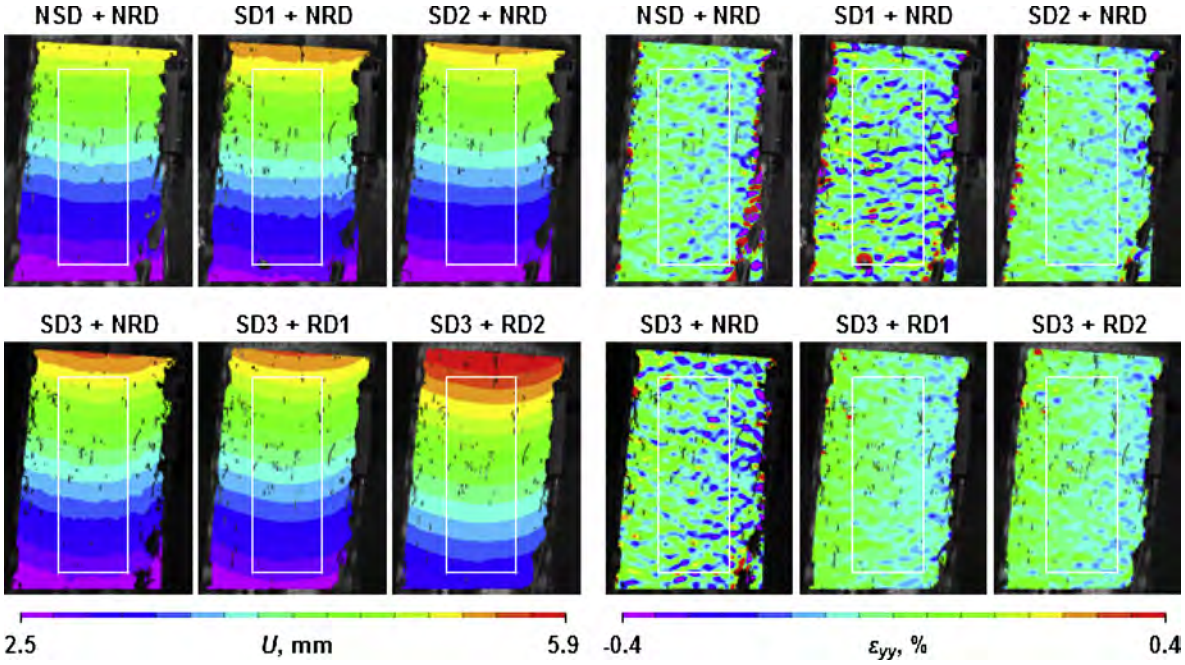

Fig. 6. Horizontal displacement field u (left) and vertical strain field ε_{yy} (right) on AoI of tree 2 for all levels of defects: no defects (NSD + NRD) and with artificially made defects at different levels on tree stem (SD1-SD3) and tree roots (RD1 and RD2). White solid rectangle represents AoI that was used for further statistics.

were loaded within returnable deformations. During the standard pulling test procedure, extensometers are not used for monitoring of the horizontal (ε_{xx}) and shear (ε_{xy}) strains because bending loading mode dominates, and, thus, they do not provide any improvement in an evaluation of tree stability. Looking at the full-field outputs of 3D-DIC also reveal that these results were shown to be less useful compared to vertical strains, similarly to Sebera et al. (2014). The role of bark is questionable, but, because bark was moderately thin and well connected to the xylem beneath (as was seen from after the failure tests), we assume that there was a good strain transfer from xylem to bark surface as reported in Dahle (2017b). The comparison of strains and displacements was carried out at force level approx. 2900 N, which diminishes doubts found in previous study (Sebera et al., 2016).

The white rectangles enclosing the AoI for subsequent data processing are shown in the form of box plots for tree 1 and tree 2 in Figs. 7 and 8, respectively. With respect to tree 1, Fig. 7 shows displacement u decreased after the first excavation (RD1) and substantially increased after the second one (RD2). The first decrease is difficult to explain and may be affected by certain measurement errors. The latter may be attributed to decreasing of the rotational stiffness of root plate caused by its greater damage. Multiple ANOVA ($\alpha = 0.05$, $n = 31096$) showed that all the groups were statistically different in the horizontal displacement, except between RD2 + NSD and RD2 + SD1 ($p = 0.27$ for null hypothesis). This means that the first stem damage (SD1) did not result in changing the mean displacement u; meanwhile, the other two subsequent damage levels (SD2 and SD3) significantly lowered mean u. This can be explained by the fact that the zone of defect started to behave more as a "joint", meaning the tree parts below and above the defect had very different deflection, so the deflection line experienced a certain breaking point. The vertical strain ε_{yy} kept increasing until 2nd damage of stem (RD2 + SD2), and then, after the last stem damage (RD2 + SD3), it decreased substantially to the level that was reached at 1st root damage and no stem damage (RD1 + NSD). It is hypothesized that the high strain occurred away from the measured AoI, so we are not able to see the "step" from our data, assuming it occurred above the defect where tree diameter is smaller than below the defect. Multiple ANOVA tests ($n = 31096$) showed that all the groups are statistically different ($p < 0.05$) except the difference between RD1 + NSD and RD2 + SD3, where p equaled 0.98 to accept a null hypothesis.

With respect to tree 2, for horizontal displacement u, the ANOVA

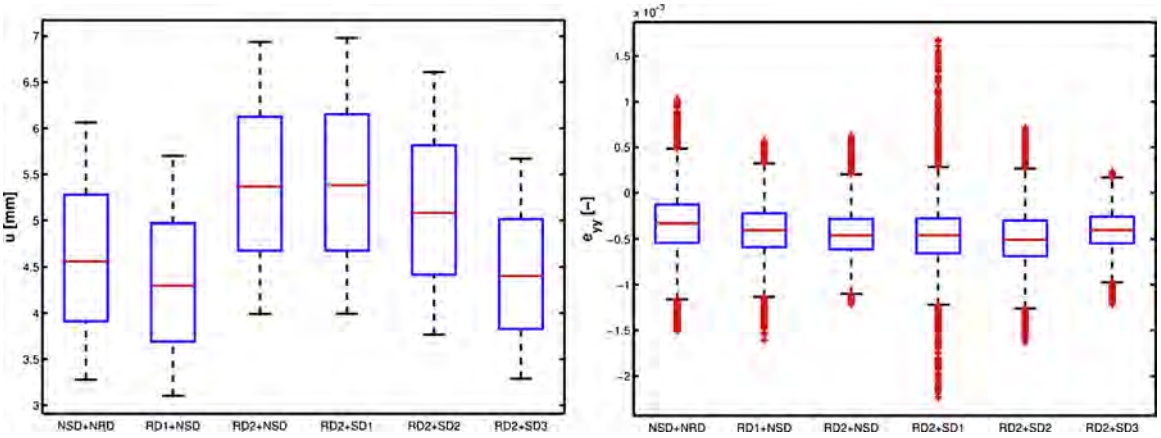

Fig. 7. Box plots for horizontal displacement fields u (left) and vertical strain ε_{yy} (right) on tree 1 made over the AoI for all levels of defects.

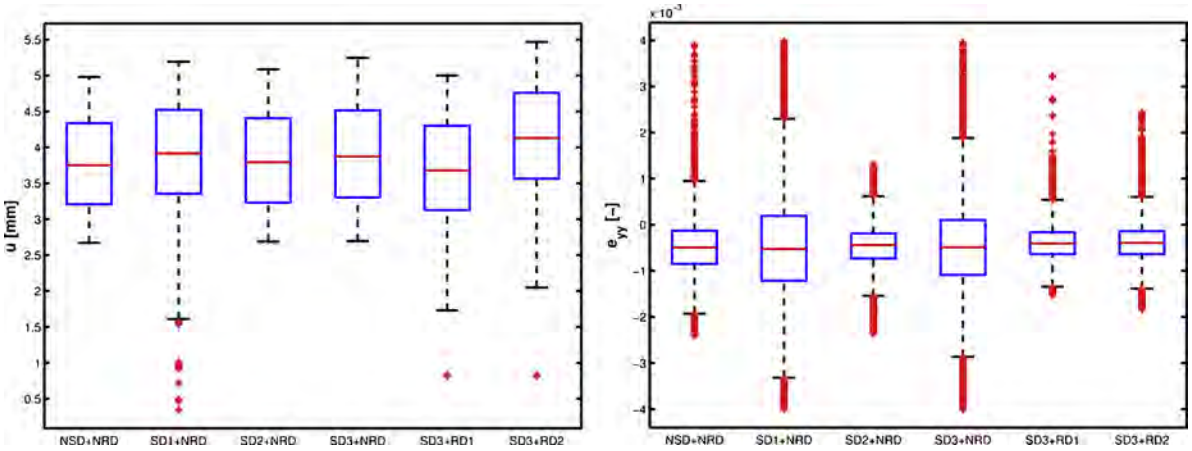

Fig. 8. Box plots for horizontal displacement u (left) and vertical strain ε_{yy} (right) on tree 2 made over the AoI for all levels of defects.

proved that all levels of defects had significantly different mean values, except comparison between NSD + NRD vs. RD1 + NSD ($p = 0.21$, $n = 36\ 366$). This suggests that most levels of damage caused significant changes to the tree system in terms of tree horizontal motion. In the case of both trees, it is necessary to say that statistical significance used in rejection or acceptance of the null hypotheses must be considered with respect to a practical significance of the tested hypotheses. As seen from Figs. 7 and 8, all data show little absolute differences amongst group means, especially from a practical measurement point of view, but because the data set is very high, the statistics show significant differences in most cases. The same statistical and practical significance conclusions also hold true when null hypothesis regarding u is based on a confidence intervals of the data.

For vertical strains ε_{yy} of tree 2, statistically significant differences were found using ANOVA ($n = 36\ 366$) amongst all groups except two comparisons: NSD + NRD vs. SD3 + NRD ($p = 0.17$) and SD3 + RD1 and SD3 + RD2 ($p = 0.98$). Similar to the displacement, the practical significance is somewhat limited for strain evaluation due to little absolute differences. It is noteworthy that although box plots do not look statistically different, one has to consider that each box plot contains a big amount of data (n), so means may be statistically different despite the box plots looking similar. The interesting phenomena for tree 2 occurred at the two last levels of damage (SD3 + RD1 and SD3 + RD2). The difference of these two levels in displacement u is the highest amongst all, meaning the 2nd root damage (RD2) significantly influenced the tree system resulting in a greater horizontal motion of the tree. Contrary to that, vertical strains ε_{yy} of both damage levels do not differ statistically, implying an AoI displaced more, but the strain increase did not occur. In general, we may state the effect of the trenching was proved using optical data. This is contrary to findings of Ghani et al. (2008), who did not find trenching as a factor decreasing anchorage rotational stiffness and turning moments in terms of statistical evidence, however, they observed decrease of these parameters. The findings of this study, however, do correspond with Smiley (2008), who found correlation among the decrease in breaking force and root cutting. The force significantly dropped (~ 20%) when over 30% of the roots were severed. More recently, Smiley et al. (2014) also found a linear relationship between number of buttress roots cut of *Acer rubrum* L. and mean bending moment that decreased as percentage of cut roots increased.

The last tests of the studied trees were carried out as destructive pulling tests until the trees' failure and, therefore, they were carried out without 3D-DIC to avoid its damage. Looking at the failure of both trees (Fig. 9), we may see that tree 1 failed by a stem breakage at defect zone; meanwhile, tree 2 was uprooted despite the extent of the defect. The failure of tree 1 was initialized on the compression side of the stem, where a compressive failure has been formed at the edge of a cut. The initial failure suggests that compressive wood properties for failure assessment are appropriate to use (Brudi and Wassenaer, 2001). Then, the failing process continued by a strong deplanation of the cross-section, which occurred as the rest wall bent inward to the defect. Then, the stem broke at the tension side on the lower edge of the defect and the tree fell down. The stem showed typical behaviour for bending. The elastic limit was reached at about 200 kN m, maximal strength of the stem was 311 kN m, which is approximately 45 MPa (stem diameter 0.41 m).

Tree 2 failed by uprooting, even though the stem damage was slightly greater than for tree 1. The failure began at the tension side of the root system, where the excavation was made. The uprooting began at the inclination of the stem base, 2.3° from where bending moment reached 259 kN m. Wessolly (1996) found that primary failure of the uprooting process begins at about 2.5°, which is slightly higher than what we measured. There could also be the influence of extensive root damage since the destructive test was carried out right after trenching. First, the stem was bent heavily with a significant curvature, but once the structural roots failed, the stem released the curvature and straightened itself. This was well documented from another camera providing images of whole tree. The force needed to move the tree decreased significantly after this moment. As the stem reached an angle of about 66.5°, the stem's own weight was so high that the root system could not carry it any longer and tree consequently fell down. Kane (2014) carried out pulling tests on 55 oak trees and reported that failure of trees, especially decurrent ones, is highly influenced by defects such as stem decay, which were simulated by stem cut outs.

Fig. 10 shows reactions of both trees in terms of applied bending moment and stem base inclination within the destructive tests. Tree 1 (black lines) shows full visco-elastic type of behavior – the stem was broken, the defect was at a weak point of the structure, therefore, the stem base inclination is significantly lower than tree 1 shows (grey lines). On the contrary, tree 2 was more compromised in the root system, so the bending moment needed for tree tipping has decreased abruptly once the structural roots failed.

Because both trees represent a limited data set, failure phenomena cannot be generalized, but, on the other hand, both illustrate the variability of trees' behavior. Even though both trees had the same location conditions (climate and soil) and both were more or less damaged in the same manner, they failed differently. This can likely be attributed to the complicated stress-strain states in a stem and root plate that we are not able to examine via performed experiments. As Peterson and Claassen (2013) showed, there is a big overlap of trees failing in breakage or uprooting, and these cannot be easily predicted based on allometric parameters. Looking at Fig. 10, the uprooted tree failed in a similar manner as described by Rahardjo et al. (2014), who numerically obtained a force-displacement curve consisting of two linear parts

Fig. 9. Failure of studied trees: a) tree 1 failing by breakage; b) tree 2 failing by uprooting.

divided by failure force. In fact, the tree failed by both shear failure of soil and breakage of main roots.

4. Conclusion

The major contribution of our study is the investigation of the possibility to use an optical technique based on 3D-DIC in identification and assessment of tree defects. The defects of concern included both root damage (trenching) and stem damage (simulating a cavity). This study further develops applicability of 3D-DIC as a part of the pulling test because it proved that it provided equivalent strains (relative difference from 5 to 13.6%) as standard and semi-destructive extensometers. The root and stem defects were identified based on 3D-DIC data with a statistical significance (on $\alpha = 0.05$) for both trees, however, the practical significance for professionals may be limited due to small differences between damaged and non-damaged states. One of the trees experienced a big change from positive to negative transversal strains, implying possible deplanation of tree cross-section – a phenomenon that needs to be investigated in further studies. The full-field data significantly improved the measurement that was based on rather discrete data from mechanical extensometers. This fact is especially important from the perspective of huge natural variability and

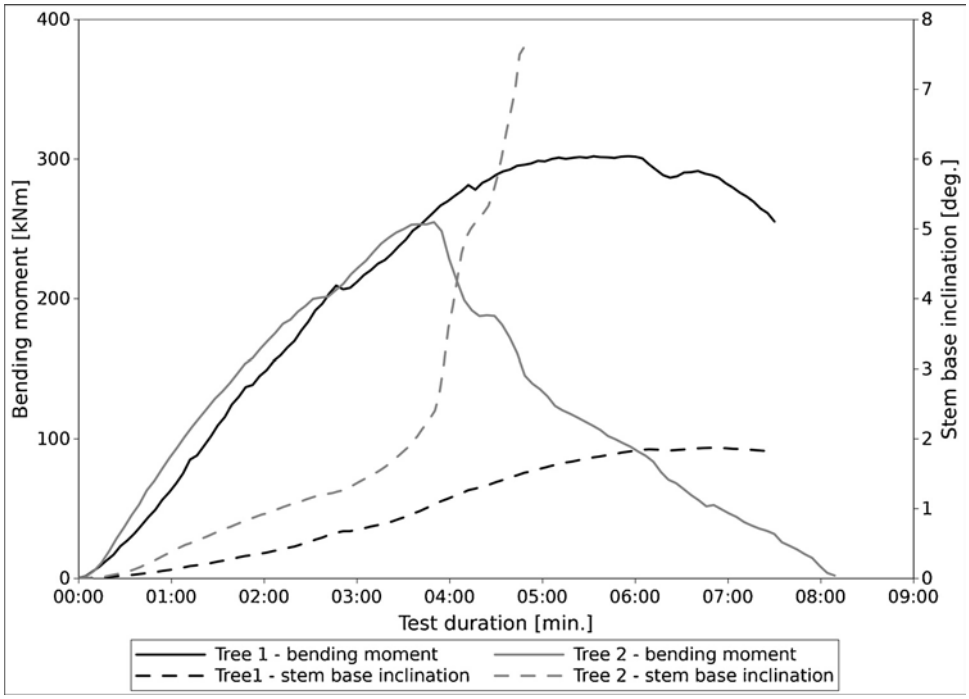

Fig. 10. Course of bending moment and stem base inclination during destructive tests of both trees. Stem base inclination was measured at the trees' neutral axis.

heterogeneity of trees and their local material properties. The tested trees were damaged in a different order of root damage and stem damage. We found that stiffness or strain evaluated at the tree may exhibit so-called path-dependent behavior, implying it depends on an order of defects' creation. Hence, it is important to know which of these two kinds of defects was created first, trenching or cavity. These findings might be useful from a practical point of view because they may help to consider the right position of extensometers, either virtual or standard ones. However, this phenomenon has to be studied on a larger sample set to confirm this finding with statistical certainty. Knowledge of defects' history may also assist in making the correct decision in tree adjustment and further interpretation of the measured data. Despite almost the same extent of artificially made defects at the end of the damage process, studied trees failed in a different manner. Because the reasoning for tree breakage and uprooting significantly overlaps in predictions, it cannot be explained by this study.

Funding

This work was supported by the Technology Agency of the Czech Republic [TA04020652], Horizon 2020 Framework Programme of the European Union; H2020 WIDESPREAD-2-Teaming: #739574 and the Republic of Slovenia, Investment funding of the Republic of Slovenia and the European Union of the European Regional Development Fund, as well as Slovenian Research Agency for funding infrastructural program IO-0035.

Declaration of Competing Interest

None.

Acknowledgement

We thank Mendel University in Brno for providing the trees for the experiments.

References

Basu, P., Pal, A., 2012. A new tool for analysis of root growth in the spatio-temporal continuum. New Phytol. 195, 264–274.
Brazee, N.J., Marra, R.E., Göcke, L., Van Wassenaer, P., 2011. Non-destructive assessment of internal decay in three hardwood species of northeastern North America using sonic and electrical impedance tomography. Forestry 84 (1), 33–39.
Brudi, E., Wassenaer, P.V., 2001. Trees and statics: nondestructive failure analysis. In: Smiley, E.T., Coder, K.D. (Eds.), Tree Structure and Mechanics Conference Proceedings: How Trees Stand up and Fall Down. ISA Publications, Savannah.
Buza, A.K., Divos, F., 2016. Root stability evaluation with non-destructive techniques. Acta Silv. Lign. Hung. 12 (2), 125–134.
Chirici, G., Bottalico, F., Giannetti, F., Del Perugia, B., Travaglini, D., Nocentini, S., Kutchartt, E., Marchi, E., Foderi, C., Fioravanti, M., Fattorini, L., Bottai, L., McRoberts, R.E., Næsset, E., Corona, P., Gozzini, B., 2018. Assessing forest windthrow damage using single-date, post-event airborne laser scanning data. Forestry 91 (1), 27–37. https://doi.org/10.1093/forestry/cpx029.
Ciftci, C., Kane, B., Brena, S.F., Arwade, S.R., 2014. Loss in moment capacity of tree stems induced by decay. Trees-Struct. Funct. 28, 517–529.
Crook, M.J., Ennos, A.R., 1996. The anchorage mechanics of deep rooted larch, Larix europea L. Japonica. J. Exp. Bot. 47, 1509–1517.
Dahle, G.A., James, K.R., Kane, B., Grabosky, J.C., Detter, A., 2017a. A review of factors that affect the static load-bearing capacity of urban trees. Arboric. Urban For. 43 (3), 89–106.
Dahle, G., 2017b. Influence of bark on the mapping of mechanical strain using digital image correlation. Wood Sci. Technol. 51 (6), 1469–1477. https://doi.org/10.1007/s00226-017-0947-0.
Detter, A., 2012. Handout for Presentation at ISA Tree Biomechanics Research Symposium Chicago 2012. 05/20/2017. http://www.tree-consult.org/index.php/171/tree-statics-and-pulling-test-method.html.
Ennos, A.R., 1995. Development of buttresses in rainforest trees: the influence of mechanical stress. In: Coutts, M.P., Grace, J. (Eds.), Wind and Trees. Cambridge University Press, pp. 293–301.
Fraser, A.I., 1962. The soil and roots as factors in tree stability. Forestry 35, 117–127.
Gao, S., Wang, X.P., Wiemann, M.C., Brashaw, B.K., Ross, R.J., Wang, L.H., 2017. A critical analysis of methods for rapid and nondestructive determination of wood density in standing trees. Ann. Forest Sci. 74, 27.
Gardiner, B., 2013. In: Gardiner, B., Schuck, A., Schelhaas, M.J., Orazio, C., Blennow, K., Nicoll, B. (Eds.), Living With Storm Damage to Forests. EFI 132 pp.
Ghani, M.A., Stokes, A., Fourcaud, T., 2008. The effect of root architecture and root loss through trenching on the anchorage of tropical urban trees (Eugenia grandis Wight). Trees-Struct. Funct. 23, 197–209.
Gryc, V., Vavrčík, H., 2009. The variability of spruce (Picea abies /L./ karst.) compression strength with present reaction wood. J. For. Sci. 55, 415–422.
James, K.R., Haritos, N., Ades, P.K., 2006. Mechanical stability of trees under dynamic loads. Am. J. Bot. 93, 1522–1530.
Kane, B., 2014. Determining parameters related to the likelihood of failure of red oak (Quercus rubra L.) from winching tests. Trees 28, 1667–1677.
Lindroth, A., Lagergren, F., Grelle, A., Klemedtsson, L., Langvall, O., Weslien, P., Tuulik, J., 2009. Storms can cause Europe-wide reduction in forest carbon sink. Glob. Change Biol. 15, 346–355.
Longuetaud, F., Mothe, F., Santenoise, P., Diop, N., Dlouha, J., Fournier, M., Deleuze, C., 2017. Patterns of within-stem variations in wood specific gravity and water content for five temperate tree species. Ann. For. Sci. 74 (3), 64.
Lundstrom, T., Jonsson, M.J., Kalberer, M., 2007. The root-soil system of Norway spruce subjected to turning moment: resistance as a function of rotation. Plant Soil 300, 35–49.
Mancuso, S., 2012. Measuring Roots: An Updated Approach. Springer-Verlag, Berlin Heidelberg.
Mattheck, C., 2004. The Face of Failure in Nature and Engineering. Forzschungszentrum Karlsruhe, Karlsruhe, Germany 196 pp.
NASA, 2013. Morton Arboretum Partners With NASA to Understand Why Trees Fail. http://www.nasa.gov/centers/glenn/technology/morton_tree.html.
Neild, S.A., Wood, C.J., 1999. Estimating stem and root-anchorage flexibility in trees. Tree Physiol. 19, 141–151.
Niklas, K.J., 1999. The mechanical role of bark. Am. J. Bot. 86, 465–469.
Niklas, K.J., Spatz, H.C., 2000. Wind-induced stresses in cherry trees: evidence against the hypothesis of constant stress levels. Trees-Struct. Funct. 14, 230–237.
Peltola, H., 2006. Mechanical stability of trees under static loads. Am. J. Bot. 93, 1501–1511.
Peters, W.H., Ranson, W.F., 1982. Digital imaging techniques in experimental stress analysis. Opt. Eng. 21, 427–431.
Peterson, C.J., Claassen, V., 2013. An evaluation of the stability of Quercus lobata and Populus fremontii on river levees assessed using static winching tests. Forestry 86 (2), 201–209.
Rahardjo, H., Harnas, F.R., Indrawan, I.G.B., Leong, E.C., Tan, P.Y., Fong, Y.K., Ow, L.F., 2014. Understanding the stability of Samanea saman trees through tree pulling, analytical calculations and numerical models. Urban For. Urban Green. 13 (2), 355–364.
Quine, C.P., 1995. Assessing the risk of wind damage to forests: practice and pitfalls. In: Coutts, M.P., Grace, J. (Eds.), Wind and Trees. Cambridge University Press, pp. 379–403.
Sani, L., Lisci, R., Moschi, M., Sarri, D., Rimediotti, M., Vieri, M., Tofanelli, S., 2012. Preliminary experiments and verification of controlled pulling tests for tree stability assessments in Mediterranean urban areas. Biosyst. Eng. 112, 218–226.
Schmidlin, T.W., 2009. Human fatalities from wind-related tree failures in the United States, 1995–2007. Nat. Hazards 50 (1), 13–25.
Schelhaas, M.J., Nabuurs, G.J., Schuck, A., 2003. Natural disturbances in the European forests in the 19th and 20th centuries. Glob. Change Biol. 9, 1620–1633.
Sebera, V., Praus, L., Tippner, J., Kunecký, J., Čepela, J., Wimmer, R., 2014. Using optical full-field measurement based on digital image correlation to measure strain on a tree subjected to mechanical load. Trees Struct. Funct. 28 (4), 1173–1184.
Sebera, V., Kunecký, J., Praus, L., Tippner, J., Horáček, P., 2016. Strain transfer from xylem to bark surface analyzed by digital image correlation. Wood Sci. Technol. 50 (4), 773–787.
Seidl, R., Schelhaas, M.J., Rammer, W., Verkerk, P.J., 2014. Increasing forest disturbances in Europe and their impact on carbon storage. Nat. Clim. Change 4, 806–810. https://doi.org/10.1038/nclimate2318.
Smiley, E.T., 2008. Root pruning and stability of young willow oak. Arboric. Urban For. 34 (2), 123–128.
Smiley, E.T., Holmes, L., Fraedrich, B.R., 2014. Pruning of buttress roots and stability changes of red maple (Acer rubrum). Arboric. Urban For. 40 (4), 230–236.
Stokes, A., 1999. Strain distribution during anchorage failure of Pinus pinaster Ait. At different ages and tree growth response to wind-induced root movement. Plant Soil 217, 17–27.
Szórádová, A., Praus, L., Kolařík, J., 2013. Evaluation of the root system resistance against failure of urban trees using principal component analysis. Biosyst. Eng. 115 (3), 244–249.
Sutton, M.A., Orteu, J.J., Schreier, H.W., 2009. Digital Image Correlation for Shape and Deformation Measurements Basic Concepts, Theory and Applications. Springer-Verlag, Heidelberg 322pp.
Wessolly, L., 1991. 2 new methods to measure the strength and stability of trees. Holz als Roh-und werkstoff 3, 99–104.
Wessolly, L., Erb, M., 2016. Manual of Tree Statics and Tree Inspection. Patzer Verlag, Berlin-Hannover 288pp.
Yan, W.M., Zhang, L., Leung, F.T.Y., Yuen, K.-V., 2016. Prediction of the root anchorage of native young plants using Bayesian inference. Urban For. Urban Green. 19, 237–252.
IPCC, 2014. Climate change 2014: synthesis report. In: Pachauri, R.K., Meyer, L.A. (Eds.), Contribution of Working Groups I, II and III to the Fifth Assessment Report of the Intergovernmental Panel on Climate Change. IPCC, Geneva, Switzerland, pp. 151 Core Writing Team.